Supplementary Information

Engineering $CoSe_2$ phase transition in Br-induced confined space for high-performance electromagnetic wave absorption

Han Ding[a], Zhihao Sun[a], Shaoyao Tian[a], Lanling Zhao[b], Lei Qian[a]*

[a]*Key Laboratory for Liquid-Solid Structural Evolution and Processing of Materials (Ministry of Education), Shandong University, 17923 Jingshi Road, Jinan 250061, China*

[b]*School of Physics, Shandong University, Jinan 250100, China*

*Corresponding author, Email address: qleric@sdu.edu.cn (Lei Qian).

Theoretical formula

With the aid of the associated dielectric loss analyzed by Debye theory, the complex dielectric constant can be expressed as:[1]

$$\varepsilon' = \varepsilon_\infty + \frac{(\varepsilon_s - \varepsilon_\infty)}{1 + (\omega\tau)^2} \quad \text{(Formula S1)}$$

To clarify the source of the sample dielectric loss, the conduction loss and polarisation loss should be analysed in detail and can be measured using the following equation:[2]

$$\varepsilon'' = \varepsilon_c'' + \varepsilon_p'' = \frac{\sigma^*}{\omega\varepsilon_0} + \frac{(\varepsilon_s - \varepsilon_\infty)\omega\tau}{1 + (\omega\tau)^2} \quad \text{(Formula S2)}$$

ε_c'' and ε_p''represent the conduction loss and polarization loss, respectively. σ* stands for electronic conductivity, while ε_0 (ε_0=8.854×10^{-12} F/m) represents the vacuum dielectric constant. τ is the relaxation time, and ω ($\omega=2\pi f$) denotes angular frequency. ε_s and ε_∞ signify static permittivity and relative permittivity at infinite frequency, respectively.

The quarter-wavelength theory($\lambda/4$) is used to explore the relationship between the matching thickness of the absorbing material (d_m) and frequency(f_m), which obeys the following equation:[3]

$$d_m = \frac{n\lambda}{4} = \frac{nc}{4f_m\sqrt{|\varepsilon_r||\mu_r|}}(n = 1,3,5\ldots) \quad \text{(Formula S3)}$$

Among them λ is the wavelength of microwave, *and c* is the speed of light in vacuum. *Z* represents the impedance matching characteristic, while the attenuation coefficient (α) can be used to evaluate the combined loss capability of the electromagnetic absorption materials. The equations for both these values are given

below:[4]

$$Z = \left|\frac{Z_{in}}{Z_0}\right| \qquad (Formula\ S4)$$

$$\alpha = \frac{\sqrt{2}\pi f}{c} \times \sqrt{\left(\mu''\varepsilon'' - \mu'\varepsilon'\right) + \sqrt{\left(\mu''\varepsilon'' - \mu'\varepsilon'\right)^2 + \left(\mu''\varepsilon' + \varepsilon''\mu'\right)^2}} \qquad (Formula\ S5)$$

Computational details

First-principles calculations: We performed the first-principles calculations in the frame of density functional theory (DFT) with the Vienna ab initio simulation package (VASP), using the Perdew-Burke-Ernzerhof (PBE) form of generalized-gradient approximation (GGA) exchange-correlation energy functional. The structure optimizations of Br doping o-$CoSe_2$/c-$CoSe_2$ and Br doping c-$CoSe_2$ have been carried out by allowing all atomic positions to vary and relaxing lattice parameters until the energy difference of successive atom configurations was less than 10-4eV. The force on each atom in the relaxed structures was less than 0.05 eV/Å. The cutoff energy for the plane-wave basis set was set to 450V. VASPKIT was used to produce K-points, and the slabs were optimized using a (1×1×2) Monkhorst-Pack grid.

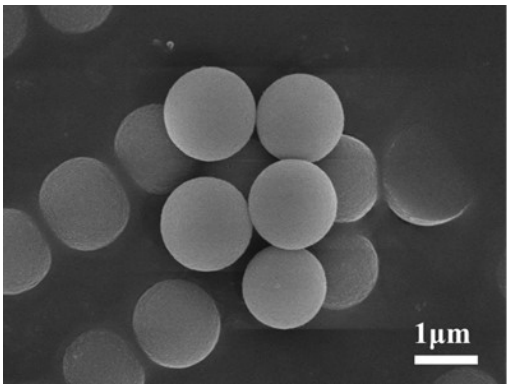

Fig.S1. FESEM images of MF.

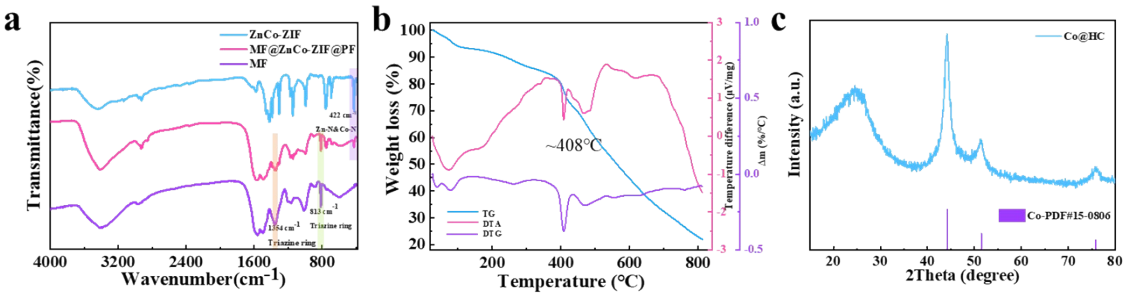

Fig.S2. (a) FT-IR spectra of ZnCo-ZIF, MF@ ZnCo-ZIF@PF and MF; (b) TG, DTA and DTG of MF@ ZnCo-ZIF@PF; (c) XRD patterns of Co@HC.

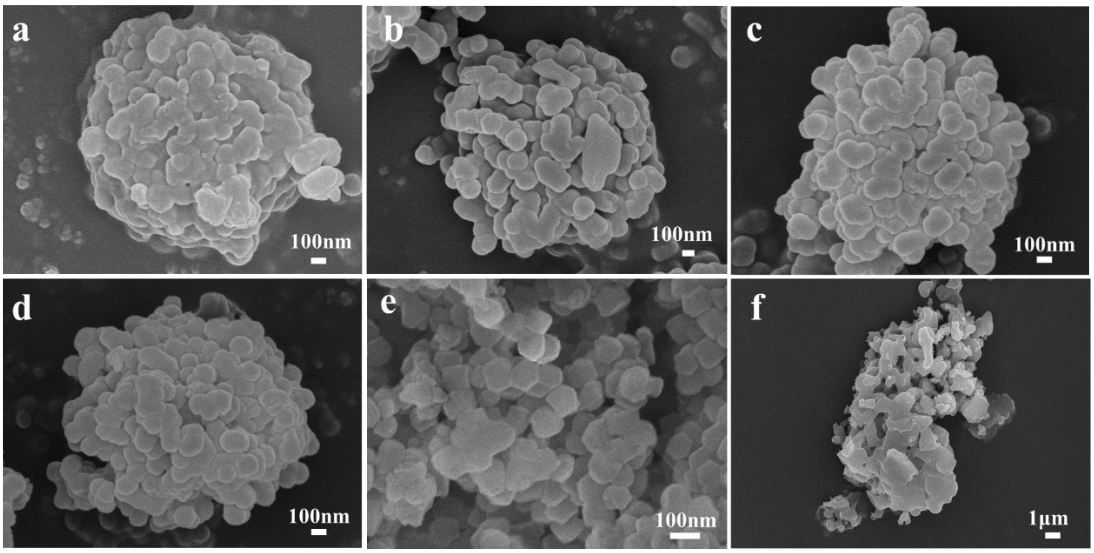

Fig. S3. FESEM images of (a) MF@ZnCo-ZIF@PF, (b) HC-Co, (c) o-$CoSe_2$@HC, (d) c-$CoSe_2$-Br_2@HC, (e) ZnCo-ZIF and (f) C@C.

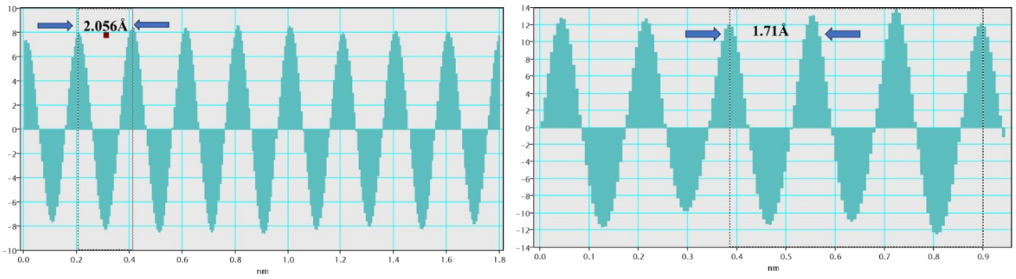

Fig.S4. Interplanar spacings of the inverse Fourier transform from o-$CoSe_2$ in o-$CoSe_2$@HC.

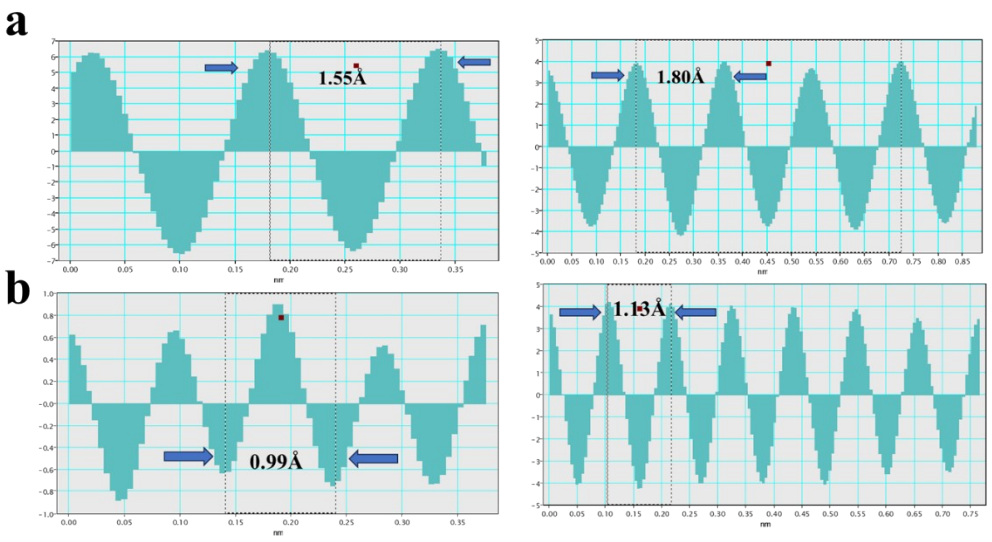

Fig.S5. Interplanar spacings of the inverse Fourier transform from (a) o-$CoSe_2$, (b) c-$CoSe_2$ in mix-$CoSe_2$-Br_1@HC.

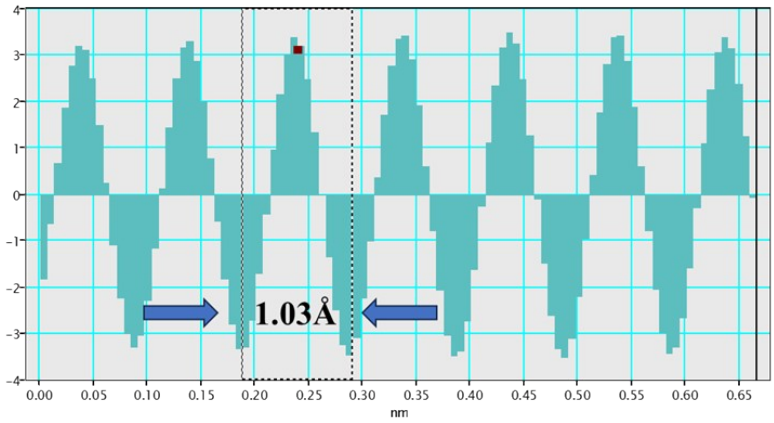

Fig.S6. Interplanar spacings of the inverse Fourier transform from c-$CoSe_2$ in c-$CoSe_2$-Br_2@HC.

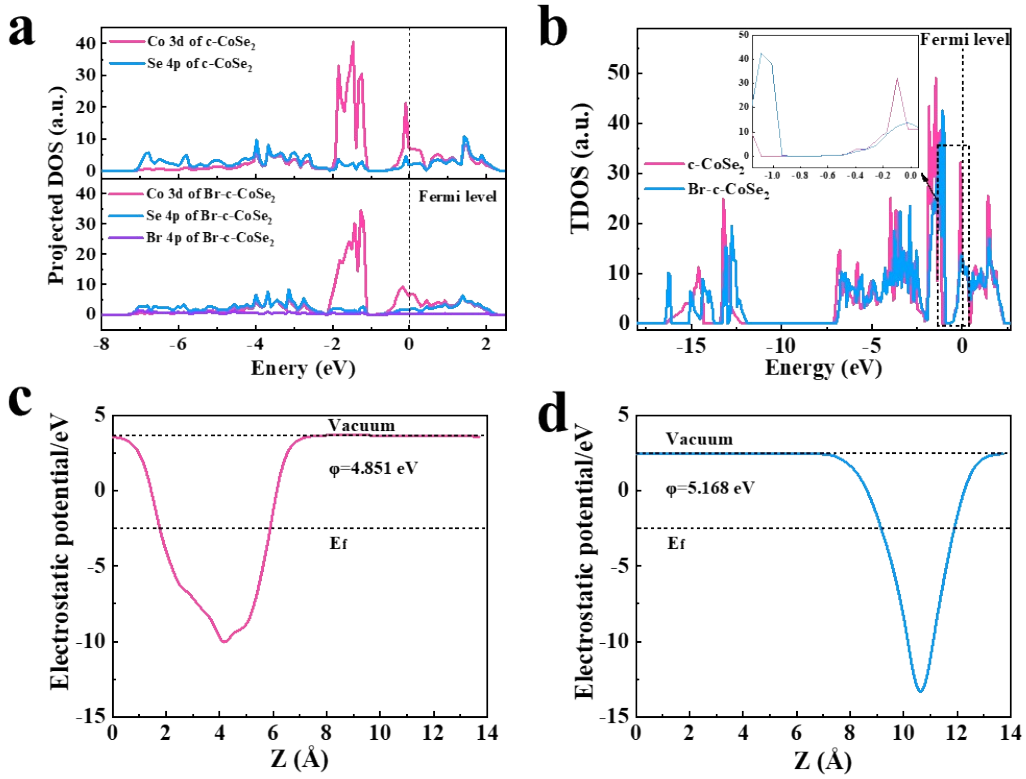

Fig.S7. (a) PDOS of c-$CoSe_2$ and Br-doped c-$CoSe_2$; (b) TDOS of c-$CoSe_2$ and Br-doped c-$CoSe_2$; (c-d) work functions of Br-doped o-$CoSe_2$ and Br-doped c-$CoSe_2$.

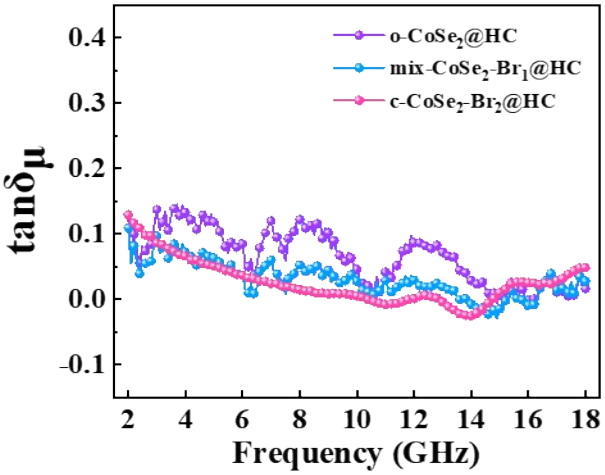

Fig.S8. Tanδ_μ of o-$CoSe_2$@HC, mix-$CoSe_2$-Br_1@HC, and c-$CoSe_2$-Br_2@ HC.

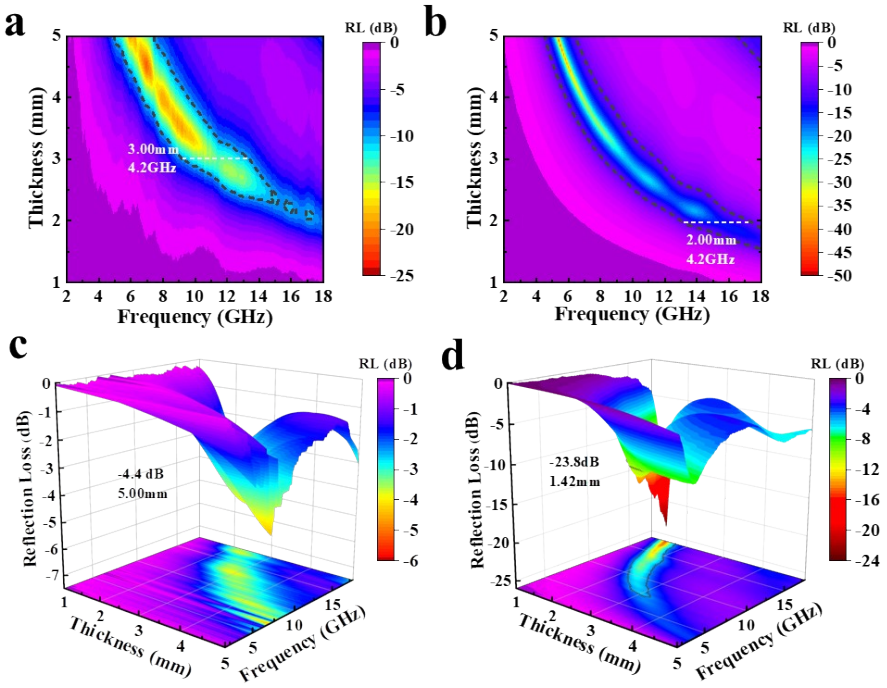

Fig.S9. (a-b) RL contour plots of o-$CoSe_2$@HC and c-$CoSe_2$-Br_2@HC; (c-d) 3D RL plots of Co@C and Co@HC.

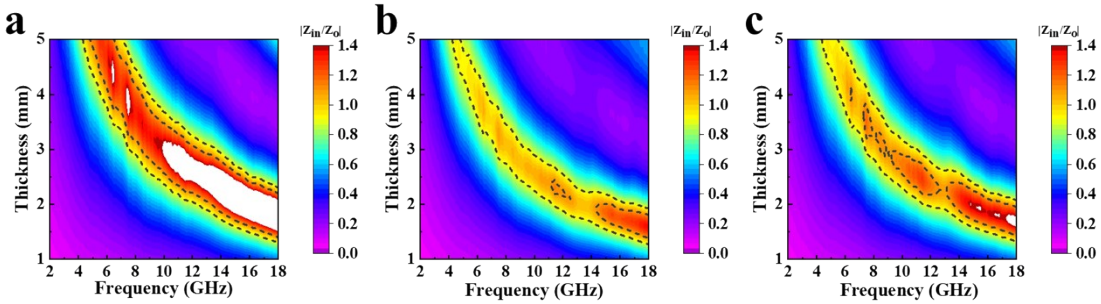

Fig.S10. 2D contour maps of $|Z_{in}/Z_0|$ of (a) o-$CoSe_2$@HC, (b) mix-$CoSe_2$-Br_1@HC and (c) c-$CoSe_2$-Br_2@HC.

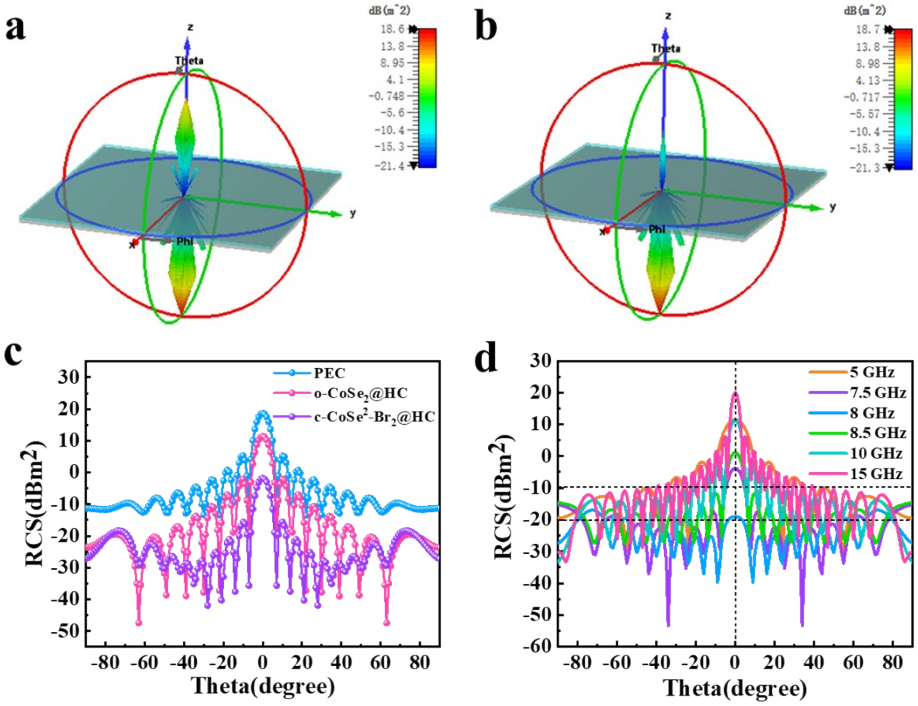

Fig.S11. (a-b) Three-dimensional radar wave scattering signals of PEC, o-$CoSe_2$@HC and c-$CoSe_2$-Br_2@ HC; (c) simulated RCS values of PEC, o-$CoSe_2$@HC and c-$CoSe_2$-Br_2@ HC under certain detecting angles; (d) the RCS curves of mix-$CoSe_2$-Br_1@HC with 3.55 mm under typical frequency in the detection range of−90°≤θ≤90°.

References

1 Z. Xu, Y. Du, D. Liu, Y. Wang, W. Ma, Y. Wang, P. Xu and X. Han, *ACS Appl. Mater.*, 2019, **11**, 4268-4277.

2 M. Zhang, H. Ling, T. Wang, Y. Jiang, G. Song, W. Zhao, L. Zhao, T. Cheng, Y. Xie, Y. Guo, W. Zhao, L. Yuan, A. Meng and Z. Li, *Nano-Micro Lett*, 2022, **14**, 157.

3 J. Tao, J. Zhou, Z. Yao, Z. Jiao, B. Wei, R. Tan and Z. Li, *Carbon*, 2021, **172**, 542-555.

4 H. Liu, X. Li, X. Zhao, M. Zhang, X. Liu, S. Yang, H. Wu and Z. Ma, *Adv. Funct. Mater.*, 2023, **33**, 2304442.